IC/94/400

INTERNATIONAL CENTRE FOR THEORETICAL PHYSICS

A NUMERICAL STUDY OF THE QUANTUM OSCILLATIONS IN MULTIPLE DANGLING RINGS

B.Y. Gu

and

Chaitali Basu

INTERNATIONAL ATOMIC ENERGY AGENCY

UNITED NATIONS EDUCATIONAL, SCIENTIFIC AND CULTURAL ORGANIZATION

MIRAMARE-TRIESTE

IC/94/400

International Atomic Energy Agency
and
United Nations Educational Scientific and Cultural Organization
INTERNATIONAL CENTRE FOR THEORETICAL PHYSICS

A NUMERICAL STUDY OF THE QUANTUM OSCILLATIONS IN MULTIPLE DANGLING RINGS

B.Y. Gu[1] and Chaitali Basu
International Centre for Theoretical Physics, Trieste, Italy.

MIRAMARE–TRIESTE
December 1994

[1] Permanent Address: Institute of Physics, Academia Sinica, P. O. Box 603, Beijing 100080, People's Republic of China and China Center of Advanced Science and Technology (World Laboratory), P. O. Box 8730, Beijing 100080, People's Republic of China.

ABSTRACT

We present the quantum mechanical calculations on magnetoconductance of the quantum waveguide topology containing multiply connected dangling mesoscopic rings with the transfer matrix approach. The profiles of the conductance as functions of the Fermi wave number of electrons and of the magnetic flux depend on the number of rings as also on the geometric configuration of the system. The conductance spectrum of this system for disordered lengths in the ring circumferences, dangling links, ballistic leads connecting consecutive dangling rings and disordered magnetic flux is examined in details. We find that there exist two kinds of mini–bands, one originating from the eigenstates of the rings, i.e. the intrinsic mini–bands, and the extra mini-bands. Some of these extra minibands are associated with the dangling links connecting the rings to the main quantum wire, while others are from the standing wave modes associated with the ballistic leads connecting adjacent dangling rings. These different kinds of mini–bands have completely different properties and responds differently to the geometric parameter fluctuations. Unlike the system of potential scatterers, this system of geometric scatterers shows complete band formations at all energies even for finite number of scatterers present. There is a preferential decay of the energy states, depending upon the type of disorder introduced. By controlling the geometric parameters, the conductance band structure of such a model can be artificially tailored and thus may guide the design of better mesoscopic switching devices.

I. Introduction

The electronic and magnetic properties of phase coherent mesoscopic structures have received much attention recently owing to the several novel phenomena observed experimentally [1–12]. Being typically of nm sizes, transport of electrons through them is in the ballistic or quasi–ballistic regimes as the phase coherence length of the electrons L_ϕ at low temperature increases significantly. When L_ϕ becomes comparable to the system size, quantum interference effects become exceedingly important. Electron transport in such systems is very similar to the microwave propagation in waveguides. The quantum interference phenomena observed and predicted in such phase coherent mesoscopic systems include the normal state Aharonov–Bohm effect in loops pierced by magnetic fields [8,9], quantized conductance in point contacts [4], Hall resistance quenching [6], Coulomb blockade and several others [7–9]. These mesoscopic systems can serve as potential quantum devices using the quantum interference phenomena[10-12].

With advances in nano–structure technology, samples of the order of electron phase coherence length L_ϕ can be fabricated with multiply connected stubs or rings. A network of many rings larger than L_ϕ has already been studied experimentally [15]. So theoretical investigation of the quantum oscillations in such multiply connected systems is relevant for a better understanding of the control in relative phase between interfering paths for their proper utilization as waveguide devices. However unlike the system studied in Ref. 15, the study of other types of structures in which the rings are located outside the main wire may also be very interesting. In this paper we carry out a detailed investigation of the dependence of the oscillatory conductance on the Fermi–wavenumber of electrons and the magnetic field piercing the loops in a system of multiple dangling loops using transfer matrix method. Here the basic building block is a dangling ring which connected to a perfectly conducting wire. As high precision scaled samples are difficult to fabricate, we introduce disorder in the lengths of the loop circumference, dangling links, interconnecting ballistic leads as also in the magnetic fields piercing the loops – to study the effect of geometric scattering in such systems. We also give a comparison of such systems with the much studied one–dimensional system of potential scatterers and show a simple way of replacing the system of geometrical scatterers by an equivalent system of

energy dependent potential scatterers.

The outline of this paper is as follows. In Section II, a model system of multiple dangling mesoscopic rings is described and the relevant formalism of transfer matrix for this particular model is presented in details. In Section III, numerical results and analyzes for fluctuations in different geometrical parameters and its effect on the magnetoconductance is pointed out. The conclusions from the observations made in section III and a summary of the work is presented in section IV.

II. Model and Theoretical treatment

A schematic representation of the quantum waveguide topology containing multiply connected dangling mesoscopic rings studied in this paper, is illustrated in Fig. 1. It consists of N rings with different circumferences $\{l_j\}$, different dangling links $\{s_j\}$ and different interconnecting ballistic leads $\{d_j\}$ between adjacent dangling structures as well as different magnetic fluxes $\{\Phi_j\}$ threading the rings. The special features of this system is that the basic building blocks are located outside the main current carrying wire. Perfectly conducting semi–infinite leads are attached on either sides of the multiple dangling–ring system at junctions 1 and N. When a potential difference is applied across the sample, these two perfect leads serve as the reservoirs of incident and transmitted electrons. Our idealization of this model to a one–dimensional quantum wire network corresponds experimentally to a network of high–mobility quantum wires with narrow width such that only the lower subband is populated. The coordinates of the points at which the dangling links are attached to the main wire are designated by x_j ($j = 1, 2, 3, ...N$) and are called the junctions. The distances between adjacent junctions are given by, $d_j = x_{j+1} - x_j$ ($j = 1, 2, 3, ...N-1$), and are allowed to be different. Coordinate s_j is the local coordinate definition of the dangling links and Φ_j is the magnetic field piercing the $j-$th ring. For simplicity our calculations use single electron approximation neglecting e–e interaction. The basic building unit of this quantum wire network is a single dangling ring connected to the perfectly conducting wire at a junction. We first derive the basic transfer matrix which relates the wave function coefficients of the electron at one side of the junction to those at the other side. The global transfer matrix that

represents the electron wave propagation through the entire device can then be obtained by cascading all the individual transfer matrices in sequence. We have used the Griffith boundary conditions at each junction owing to the requirement of the single valuedness of wave functions and the conservation of the current density (Kirchoff's law) [3,14,18]. For example, at the junction x_j we have

$$\psi_1(x_j) = \psi_2(x_j) = \psi_3(x_j), \tag{1a}$$

and

$$\sum_{i=1}^{3} \frac{d\psi_i}{dx} \mid_{x_j} = 0, \tag{1b}$$

where ψ_1, ψ_2, and ψ_3 represent the electron wave functions in the left-side lead of the junction, the dangling link and the right-side lead of the junction respectively. All the derivatives are either outwards or inwards from the junction.

First, we need to derive the wave function of the dangling ring by considering the $j-$th node at which the $j-$th ring is connected to the $j-$th dangling link. Consider an electron with the wave number k and energy $\epsilon(k) = \hbar^2 k^2/2m^*$ propagating through the $j-$th ring. m^* is the effective mass of the electron. In the presence of a magnetic field piercing the ring, we can write the wavefunctions at the $j-$th node as [3]

$$\psi_{link} = a_1 e^{ik(y-s_j)} + a_2 e^{-ik(y-s_j)}, \tag{2a}$$

for the dangling link, where y is the local coordinate along the link.

$$\psi_l = b_1 e^{ik_1 z} + b_2 e^{-ik_2 z}, \tag{2b}$$

for the electron wave moving in the left arm of the ring,

$$\psi_r = c_1 e^{ik_2 z} + c_2 e^{-ik_1 z}, \tag{2c}$$

for the electron wave moving in the right arm of the ring. z is the local coordinate definition in the loop. Here we have used symmetric gauge for the vector potential of the magnetic field $\mathbf{B_j}$, i.e. $A_j = \Phi_j/l_j$, $\Phi_j = B_j S_j$ is the magnetic flux through the ring section area S_j, and l_j is the circumference of the ring. k_1 and k_2 are related to k by

$$k_1 = k + \frac{e\Phi_j}{\hbar c l_j} = k + \frac{\theta_j}{l_j},$$

$$k_2 = k - \frac{e\Phi_j}{\hbar c l_j} = k - \frac{\theta_j}{l_j},$$

and

$$\theta_j = \frac{2\pi\Phi_j}{\Phi_0}, \quad \Phi_0 = \frac{hc}{e},$$

Φ_0 is the elementary flux quantum. Using Griffith boundary conditions at the node of the ring and with the periodic boundary conditions prevailing in the ring, we get

$$b_1 e^{ik_1 l_j} = c_2, \tag{3a}$$

$$b_2 e^{-ik_2 l_j} = c_1, \tag{3b}$$

$$a_1 + a_2 = b_1 + b_2 = c_1 + c_2, \tag{3c}$$

$$k(a_1 - a_2) = k_1 b_1 - k_2 b_2 + k_2 c_1 - k_1 c_2. \tag{3d}$$

With the standard algebraic manipulations we can find the relation between the coefficients a_1 and a_2 as follows :

$$\frac{a_2}{a_1} = e^{i2\xi(kl_j)} = \frac{2(\cos(kl_j) - \cos\theta) + i\sin(kl_j)}{-2(\cos(kl_j) - \cos\theta) + i\sin(kl_j)}. \tag{4}$$

As seen a_2/a_1 is a phasor with modulus 1. The form of the wave function in the dangling ring can be expressed as

$$\psi_2 = 2a_1 e^{i\xi(kl_j)} \cos(k(y - s_j) - \xi(kl_j)) = p\cos(k(y - s_j) - \xi(kl_j)). \tag{5}$$

We now derive the transfer matrix for the $j-$th junction in the main wire. The corresponding wave functions are

$$\psi_1 = f_1 e^{ik(x-x_j)} + f_2 e^{-ik(x-x_j)},$$

$$\psi_2 = p\cos(k(y - s_j) - \xi(kl_j)), \tag{6}$$

$$\psi_3 = g_1 e^{ik(x-x_j)} + g_2 e^{-ik(x-x_j)}.$$

Using the Griffith boundary conditions at the $j-$th junction, we obtain the transfer matrix connecting the coefficients $\{g_1 e^{-ikx_j}, g_2 e^{ikx_j}\}$ and $\{f_1 e^{-ikx_j}, f_2 e^{ikx_j}\}$ as

$$\widehat{M}(kx_j) = \widehat{U}^{-1}(ikx_j)\widehat{m}(kl_j)\widehat{U}(ikx_j),$$

where

$$\widehat{m}(kl_i) = \begin{pmatrix} 1 + i0.5\tan(ks_j + \xi(kl_j)) & i0.5\tan(ks_j + \xi(kl_j)) \\ -i0.5\tan(ks_j + \xi(kl_j)) & 1 - i0.5\tan(ks_j + \xi(kl_j)) \end{pmatrix} \quad (7)$$

and

$$\widehat{U}(\eta) = \begin{pmatrix} e^{\eta} & 0 \\ 0 & e^{-\eta} \end{pmatrix}.$$

The global transfer matrix can be constructed as the product of the individual transfer matrices associated with each junction in order. Thus we obtain

$$\widehat{M}_{tot} = \widehat{U}^{-1}(ikx_N)\widehat{m}(kl_N)[\Pi_{j=1}^{N-1}\widehat{U}(ik(x_{j+1} - x_j))\widehat{m}(kl_j)]\widehat{U}(ikx_1). \quad (8)$$

The transmission amplitude of the electrons is related to the element of $\widehat{M}_{tot}$ as $t(k) = 1/M_{tot}(2,2)$. For a given configuration of a network of the dangling rings, we carry out the matrix multiplication. The two–terminal dimensionless conductance g of the device at small voltages can be written using Landauer's formula [18,19] as,

$$g = G/(\frac{2e^2}{h}) = \mid t \mid^2 . \quad (9)$$

III. Numerical Results and Analyzes

In Fig. 2a, we plot the two terminal conductance as a function of the scaled Fermi wave-number of the electron in a single ring system with and without the dangling link. Curve a shows the case when there is no dangling link and the ring is directly attached to the main wire. The junction formed on the main wire is a four-way junction with the electron wave having four alternative paths of travel. With proper modifications of the boundary condition, we find the conductance oscillates between 0 and 1 with a regular periodicity. The eigen states of the ring determined by the condition $e^{ikl_0 l} = 1$, give rise to transmission unity for those values of the Fermi wave-number at which $kl_0 l = 2n\pi$. Here all lengths are measured in units of l_0 and are hence dimensionless. With $l = 1$, we find conductance peaks at $kl_0/\pi = 0, 2, 4, ...,$. With introduction of a finite dangling link, the electron wave at the junction has three channels for transport. However here, apart from the eigen states of the ring, a standing wave pattern is formed in the dangling link which interferes with the plane wave in the main wire. This gives rise to transmission peaks and zeros at more energy points. If we refer to the

peaks of curve a as the intrinsic peaks of the ring, then apart from these intrinsic peaks, we find some extra peaks appearing in the conductance pattern of curve b. With introduction of the dangling link, apart from the intrinsic peaks becoming narrower, two extra peaks appear in between the intrinsic peaks. These extra peaks come from the interference of the standing waves of the dangling links and are attributed to the specific parameters of the link. In both curves ring circumference $l_1 = 1$ and in curve b, length of the dangling link $s_1 = 1$.

In Fig. 2b, we study the same effect for a two ring system. Curve a shows the conductance of a system of two rings attached directly to the main wire. As in serially connected stub and loop systems [13,14,17], we also find clear band formation in curve a. Each intrinsic peak gives rise to 2N–1 (where N is the number of rings, here N=2) resonances. This behavior is very similar to superlattice structures where each band gives rise to N–1 resonances. Here circumferences $l_j = 1$ and ballistic lead $d_1 = 1$. As we increase the length of the ballistic leads ($d_1 = 1.5$ for curve b), we find the appearance of sharp resonant peaks in between the allowed bands. This arises because of a change in the standing wave pattern in the ballistic leads. With a further increase of $d_1 = 2.5$ in curve c, the number of sharp resonant peaks increase and the intrinsic bands become narrower. In all the three curves discussed $a - c$, the junctions are four–way junctions. As dangling links are attached to both rings, we find the appearance of extra bands (curve d). Each of the intrinsic bands give rise to 2N–1 resonance spikes and the extra bands tend to widen as the standing waves in the dangling links interfere with those in the ballistic leads. With increase in the ballistic lead length from $d_j = 1$ in curve d to $d_j = 1.5$ in curve e and $d_j = 2.5$ in curve f, we find noticeable change in the structure of the extra bands with sharpening of band edges and appearance of oscillatory structures in them. So a multi–dangling ring structure gives rise to complete band structures formation. Of these, the intrinsic bands are peculiar to the rings and the extra peaks are formed entirely due to the interfering standing waves of the dangling link and the ballistic leads.

We now look into the effect of a change in the length of the ring circumference on the conductance profile. In Fig. 3, we plot conductance g versus scaled Fermi-wavenumber for a system of three rings. Curve a shows for an ordered system

with l_j =1, s_j =1 and d_j =1. As seen, for this system, there are the flatter extra bands and the oscillatory intrinsic bands with 2N−1 (N=3) resonances. These intrinsic peaks occur at the positions of cavity resonances and satisfy the condition : $kl_0l = 2n\pi$. So at $l = 1$, the intrinsic peaks occur only at $kl_0/\pi = 0, 2, 4$ as seen in curve a. If $l = 1.5$, as is the case for curve b, the positions of the intrinsic peaks are at $kl_0/\pi = 0, 4/3, 8/3, 4$. So in curve b, we find the intrinsic peaks at 0 and 4 remaining the same, while that at 2 disappears with new bands appearing at 4/3 and 8/3. These new bands are much ill-formed as compared with the well formed bands at kl_0/π =0 and 4. This is because of a mixing of the modes of the eigenstates of the ring and the standing waves of the dangling links at those energies where the new bands appear. Introducing asymmetry into this system with $l_1 = l_3$ =1.5 and l_2 =1, we find an enhanced effect of this mode mixing. Now there are two different sets of allowed modes in the rings corresponding to the different values of circumference parameters and an increase in the out of phase interference of the waves at the junctions causes a destruction of the band formations making the conductance profile highly oscillatory. So at zero field, in a system of multiply connected ordered dangling rings, we can clearly distinguish the intrinsic bands which are formed when the electron energy coincides with the eigen energy of the rings while the extra bands come from the standing waves in the dangling links and the ballistic leads. However some of the allowed modes of the standing wave in the wires may overlap with the intrinsic bands making it broader.

In Fig. 4 we plot conductance g versus kl_0/π with increasing number of dangling rings. Curves a – e correspond to systems with 1, 2, 3, 5 and 12 dangling rings respectively. With increase in the number of dangling rings, the resonances in the intrinsic bands become sharper with their widths varying as $1/N$ and the band edges are also sharpened. The flatter extra bands develop oscillatory structures because of an increase of the junction scatterings in the main wire. Unlike a system of potential scatterers, the presence of a few of these geometric scatterers, typically of the order of 3, can generate the complete band structure for all the values of the Fermi wavenumbers.

We now introduce a magnetic field and study the effect of increasing the magnetic flux threading the rings on the conductance profile. In Fig. 5 we

plot, magnetoconductance g vrs kl_0/π for a single dangling ring attached to two electron reservoirs. Curves $a - f$ correspond to θ = 0.0, 0.2π, 0.4π, 0.6π, 0.8π and 1.0π respectively. Magnetic field lifts the degeneracy of the eigenstates in the ring and this causes each of the intrinsic bands to split into two bands. With increase in θ values, these split bands move apart. A decrease in conductance at some k values is compensated by an increase in conductance at some other k values. At θ =1.0π (curve f), the band structure is same as in curve a for θ =0 with a steady shift to higher energy region. The effect of increasing field on the band structure is periodic in θ with a period π. As the magnetic field only introduces a phase difference between the interfering waves at the ring nodes, it is expected that only the intrinsic bands due to the rings will be affected. This also strengthens our belief that the intrinsic bands are formed entirely by the eigenstates of the rings.

In Fig. 6, we study the magnetoconductance g vrs θ/π at a fixed Fermi-energy with increasing number of dangling rings (N). We fix the Fermi wavenumber at $kl_0 = 0.608\pi$ at which the peak of an extra band occurs. Curves $a - e$ correspond to N=1, 2, 5, 8 and 12 respectively. As seen, with increase in N, the bands develop and for N typically of the order of 5, complete band formation with sharp band edges appear. The conductance profile for kl_0 fixed at values at which other peaks appear (for instance, at 0.2π for 1st intrinsic band and 1.39π for the 2nd extra band), behaves in a similar manner with increasing number of dangling rings.

The difficulty in making highly precision scaled samples makes the study of disorder in geometric parameters of the system extremely essential. The degree of parameter precision required for the system to remain conducting is investigated in Fig. 7. We plot the ensemble-averaged conductance $< g >$ vrs kl_0/π with increasing disorder in the different geometric parameters for a system of 20 dangling rings. The averaging is taken typically over 1200 configurations which is sufficient to ensure stability and convergence. In Fig. 7a we introduce disorder only in the circumference of the loop, keeping all $s_j = 1$ and $d_j = 1.5$. Curves $a - e$ correspond to w_c =0.0, 0.1, 0.2, 0.3 and 0.4 respectively. We calculate circumferences l_j as

$$l_j = (1 + R_j.w_c).l_0$$

w_c is the disorder parameter for ring circumference. Disorder in circumference causes a decay in the intrinsic bands much faster than a decay in the extra bands. However there is an overall decay of conductance for all the energy states with a faster decay in some than in the others. As electrons with higher energies have shorter wavelengths, geometric parameter fluctuations in a small system (here it is of the order of 20) is seen by it while electrons with smaller values of kl_0 will not feel any effect of the parameter fluctuations at all. So the peak around kl_0 =0 do not show any decaying tendency.

Fig. 7b shows the same for disordered dangling links and the circumferences l_j =1 and the ballistic leads d_j =1.5. We calculate the dangling link lengths as

$$s_j = (1 + R_j.w_s).l_0$$

w_s is the disorder parameter for the dangling link. Curves $a - e$ correspond to w_s = 0.0, 0.1, 0.15, 0.2 and 0.25 respectively. With increase in w_s, the extra peaks are more affected than the intrinsic peaks with an overall decay in conductance of all energy states. But as can be seen, a disorder in the dangling links destroy the band structure much faster than the circumference disorder. As the ring is located outside the main path of the electron current flow, a change in the geometric parameter of the ring has only an indirect effect on the current flow in the main wire, while the dangling links being directly attached to the junctions of the main wire has a stronger effect on the allowed modes of the standing wave formed in the main wire.

Fig. 7c shows the same for a disorder in the ballistic leads. So the junctions of the main wire do not appear periodically. The interval between adjacent junctions are given by

$$d_j = x_{j+1} - x_j$$

with disorder introduced in d_j as

$$d_j = (1 + R_j.w_d).l_0$$

w_d is the disorder parameter for the ballistic leads. Curves $a - e$ correspond to w_d =0.0, 0.1, 0.15, 0.2 and 0.25 respectively. With increase in disorder, the forward and backward scattering waves at the junctions interfere increasingly,

and this leads to a sharpening of the intrinsic bands. A partial decay of some of the extra bands start in curve b at $w_d = 0.1$. With increase in w_d, the extra bands originating from the allowed modes of the waves in the ballistic leads decay completely while resonant states due to the rings (intrinsic bands) and the dangling links (extra bands) are unaffected. Unlike the system of potential scatterers, where all states get localized with introduction of an infinitesimal disorder in one-dimension (except for the presence of some stochastic resonances), this system of geometric scatterers have some states conducting even with the introduction of positional disorder for the scatterers.

¿From Figs. 7(b) and 7(c), we could clearly distinguish the bands due to the ballistic leads from the bands due to the dangling links. So the three length scales involved in the system seem to give rise to different allowed energy regions in the band structure making the study of such systems of geometric scatterers comparatively simpler. The very different behavior of the geometric scatterers from the potential scatterers can be understood if we consider the following model systems :

(1) A system of δ–function potential scatterers of potentials $V_0\delta(x)$ which is attached to perfectly conducting semi-infinite leads on either side.

(2) A system of many dangling rings attached to junctions placed periodically on a wire. Perfectly conducting semi-infinite leads are attached on either side of this wire.

Using transfer matrix approach, we can obtain the matrix relating coefficients of the wavefunction on either side of a single scatterer or a single junction as

$$\widehat{m}(k) = \begin{pmatrix} 1 - i0.5\Omega/k & -i0.5\Omega/k \\ i0.5\Omega/k & 1 + i0.5\Omega/k \end{pmatrix}$$

For case (1) (the potential scatterer system), the form of $\Omega = 2m^*V_0/\hbar^2$, where m^* is the effective mass of the electron. For case (2) (the geometric scatterer system), the form of $\Omega = -k\tan(kd + \xi(kl_0l)$ (see equation (7)). Comparing these expressions of Ω, we find that if the constant potential V_0 is replaced by an energy dependent complex function, then the scattering in both systems are equivalent. In this case

$$V_0 = \frac{\hbar^2}{2m^*}[-k\tan(kd + \xi(kl_0l))] = V_0(k)$$

Therefore, it turns out that the system of geometric scatterers can be mapped on an equivalent system of potential scatterers where the constant scattering potential is replaced by an amplitude modulated complex periodic function of the electron energy. It is this energy dependent potential amplitude that gives rise to such different characteristics in the systems of geometric and potential scatterers.

VI. Conclusion

We have presented the magnetoconductance profile study for the multiple dangling ring system connected to ballistic leads for different values of the Fermi wave number of electrons. This model device involves three periodic length scales, namely, the ring circumference, the dangling links and the connecting ballistic lead lengths. We found that periodic miniband structures are formed with increase in the number of rings. There are two types of minibands – one due to the eigenstates of the rings while the second due to the standing wave modes in the dangling links and in the the ballistic leads. These two types of minibands behave differently in response to external perturbations. Change in periodicity of any one length scale alters only the corresponding mini-bands keeping the others intact. Asymptotically both geometric scatterers and potential scatterers localizes all energy states exponentially. However in the mesoscopic regime, for the system of geometric scatterers, disorder in any one of the length scales involved in the system tends to cause preferential localization in a band of energy states. This is never the case for the potential scatterers. These characteristics of the geometric scatterers are very different from the one-dimensional δ-function potential scatterer system. However, we find that this system of geometric scatterers can in effect be mapped onto a system of δ-function potential scatterers with the constant amplitude of the δ-function potentials replaced by an energy dependent complex periodic function. By controlling and tuning the geometric parameters of the model devices, the conductance band structures may be artificially tailored to meet the desired effect and can guide the design of new mesoscopic devices.

The effect caused by the geometric scattering and the competing periodicities of the different length scales involved in the system is of a much general

nature and we expect this to be true for all nano-structure devices involving more that one length scale. This may have far reaching consequences in the working of devices which use interferometric principle.

ACKNOWLEDGMENTS

One of the authors (B. Y. Gu) would like to thank Professor Abdus Salam, the International Atomic Energy Agency and UNESCO for hospitality at the International Centre for Theoretical Physics, Trieste.

REFERENCES

1. Pfeiffer, L., West, K.W., Stormer, H.L., Eisenstein, J.P., Baldwin, K.W., Gershoni, D., and Spector, J., : Appl. Phys. Lett. **56**, 1697 (1990)
2. In : The Physics and Fabrication of Microstructure and Microdevices. Kelly, M.J., and Weisbuch, C. (eds.). Berlin: Springer–Verlag 1986; In : Nanostructure Physics and Fabrication. Reed, M.A., Kirk, W.P. (eds.). New York : Academic 1989; In : Physics and Technology of Submicron Structures. Heinrich, H., Bauer, G., Kuchar, F. (eds.). New York : Springer–Verlag 1988
3. Xia, J. B. : Phys. Rev. **B45**, 3593 (1992)
4. Van Wees, B.J., Van Houten, H., Beenakker, C. W. J., Williamson, J.G., Kouwenhoven, L.P., Van der Marel, D., Foxson, C.T. : Phys. Rev. Lett. **60**, 848 (1988); Van Wees, B.J., Kouwenhoven, L.P., Willems, E.M.M., Harmans, C.J.P.M., Mooij, J.E., Van Hauten, H., Beenakker, C.W.J., Williamson, J.G., Foxon, C.T. : Phys. Rev. **B43**, 12431 (1991); Wharam, D.A., Thornton, T.J., Newbury, R., Pepper, M., Richie, H., Jones, G.A.C. : J. Phys. **C21**, L209 (1988).
5. Weiss, D. : In : Electronic Properties of Multilayers and Low Dimensional Semiconductor Structures. Chamberlain, J.M., Eaves, L., Portal, J.C. (eds.). New York : Plenum 1990
6. Roukes, M.K., Scherer, A., Allen, S.J., Craighead, H.G., Ruthen, R.M., Beebe, E.D., Harbinson, J.P. : Phys. Rev. Lett. **59**, 3011 (1987)
7. In : Quantum Coherence in Mesoscopic Systems, Vol **254**, NATO ASI Series B ,-- Physics. Kramer, B. (ed.). New York : Plenum, 1991; In : Mesoscopic Phenomenon in Solids. Altshuler, B.L., Lee, P.A., Webb, R.A. (eds.). Amsterdam : North–Holland, 1991; Beenakker, C.W.J., Van Houten, H. : In : Solid State Physics – Semiconductor Heterostructures and Nanostructures. Ehrenreich. H., Turnbull, D. (eds.). New York : Academic, 1991
8. Washburn, S., Webb, R.A. : Adv. Phys. **35**, 75 (1986); Webb, R., Washburn, S., Umbach, C., Laibowitz, R. : Phys.Rev. Lett. **54** , 2696 (1985); Chandrashekhar, V., Rooks, M., Wind, S., Prober, D. : *ibid.* **55**, 1610 (1985); Datta, S., Melloch, M., Bandyopadhyay, S., Noren, R., Vaziri, M., Miller, M., Reifenberger, R. : *ibid.* **55**, 2344 (1985)
9. Gefen, Y., Imry, Y., Azbel, M. : Phys. Rev. Lett. **52**, 129 (1984); Kumar, N., Jayannavar, A.M. : Phys. Rev., **B32**, 3345 (1985) ; Browne, D.A., Carini, J.P., Nagel, S.R. : Phys. Rev. Lett. **55**, 136 (1985); Landauer, R., Buttiker, M. : *ibid.* **54**, 2049 (1985); Stone, A.D., Imry, Y. : *ibid.* **56**, 189 (1986)
10. Sols, F., Macucci, M., Ravoili, V., Hess, K. : Appl. Phys. Lett. **54**, 350 (1990); J. Appl. Phys. **66**, 3892 (1989); Jaynnavar, A.M., Singha Deo, P. : Mod. Phys. Lett. **B8**, 301 (1994)
11. Landauer, R. : Physics Today **42**, No. 109, 119 (1989)
12. Subramaniam, S., Bandopadhyay, S., Porod, W. : J. Appl. Phys. **68**, 4861 (1990)
13. Takai, D., Ohta, K. : Phys. Rev. **B50**, 2685 (1994)
14. Singha Deo, P., Jayannavar, A. M. : Phys. Rev. **B50**, 11629 (1994)
15. Umbach, C.P., Haesendonck, C.V., Laibowitz, R.B., Washburn, S., Webb, R.A. : Phys. Rev. Lett. **56**, 386 (1986)
16. Buttiker, M. : Phys. Rev. **B32**, 1846 (1985); Jayannavar, A.M., Singha Deo, P. : Phys. Rev. **B49**, 13685 (1994)
17. Basu, C., Gu, B. Y. (unpublished)
18. Landauer, R. : Z. Phys. **B68**, 217 (1987); J. Phys. Condens.
19. Buttiker, M., Imry, Y., Landauer, R., Pinhas, S. : Phys. Rev. **B31**, 6207 (1985)

FIGURE CAPTIONS

FIG. 1 Schematic representation of a multiple dangling–ring system inter–connected by ballistic leads. The circumference of the loops are l_j (j=1,2,3..,N) and the dangling links are s_j. The positions of the junctions on the main current carrying wire are designated by x_j with the distance between two junctions (which is also the length of the ballistic leads) given by $d_j = x_{j+1} - x_j$. The magnetic flux threading the loops are given by Φ_j.

FIG. 2 Conductance g versus the scaled Fermi wave-number kl_0/π for (a) a single ring system, without the dangling (curve a) and with the dangling link (curve b). The junction for the first case is a four–way junction while that for the second case is a three–way junction. For both curves $l_1 = 1$ and for curve b, $s_1 = 1$. Curve b is vertically shifted for clarity, (b) for a system of 2 rings for different ballistic lead lengths. Curves $a - c$ correspond to the system of rings attached directly to the main wire (*i.e.* s_j =0). Curves $d - f$ correspond to the system of finite dangling links which connected the rings to the main wire. In all the cases $l_j = 1$ and for curves $d - f$, $s_j = 1$. The ballistic leads parameters for curves a and d are $d_1 = 1$, for curves b and e are $d_1 = 1.5$ and for curves c and f are $d_i = 2.5$. The curves $b - f$ are vertically shifted for clarity.

FIG. 3 Conductance g as a function of scaled Fermi wavenumber kl_0/π for a system of 3 rings with differing circumference parameters. For all the curves $s_j = d_j = 1$. Curve a has $l_j = 1$, curve b has $l_j = 1.5$ and curve c has $l_1 = l_3 = 1.5$ and $l_2 = 1$. The last curve corresponds to an asymmetric system. Curves b and c are shifted vertically for clarity.

FIG. 4 Oscillatory conductance g versus scaled Fermi wave-number kl_0/π with increasing number of dangling rings. Curves a–e show number of rings increasing from 1, 2, 3, 5 and 12 respectively. Note the band structure formation for the system of typically 3 dangling rings. For all curves $l_j = s_j = d_j = 1.0$ (i.e. system is ordered).

FIG. 5 Magnetoconductance g as a function of the scaled Fermi wave number kl_0/π, for a single dangling ring, with increasing magnitude of the flux threading the loops. Curves $a - f$ correspond to increasing values of θ =0.0, 0.2π, 0.4π, 0.6π, 0.8π and 1.0π. Note that curves a and f are the same with a continuous shift in the energy scale. For all the curves $d_j = s_j = l_j = 1$.

FIG. 6 Magnetoconductance g as a function of θ/π at $kl_0 = 0.608\pi$ for increasing number of dangling rings N. Curves $a - e$ corresponds to N = 1, 2, 5, 8 and 12 respectively. Curves are vertically shifted for clarity.

FIG. 7 The averaged value of conductance, $< g >$ plotted as a function of scaled Fermi wave–number kl_0/π for a system of 20 rings. (a) At zero field for increasing circumference disorder w_c=0.0, 0.1, 0.2, 0.3 and 0.4 (curves a–e), (b) At zero field for dangling link disorder w_s = 0.0, 0.1, 0.15, 0.2 and 0.25 (curves $a - f$), (c) At zero field for ballistic lead disorder w_d = 0.0, 0.1, 0.15, 0.2 and 0.25 (curves $a - e$) and (d) For ordered geometric parameters and disorder in the magnetic flux threading the loops. The disorder is w_f=0.0, 0.1, 0.2, 0.4 and 0.6 (curves $a - e$). The minibands due to the loops split in two due to breaking to time reversal symmetry. The low energy electrons are affected only when the magnetic field is turned on.

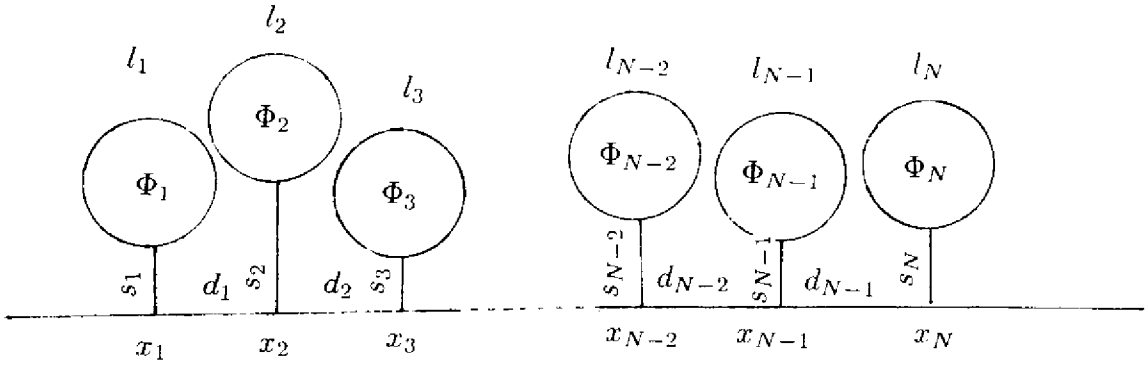
l_1
l_2
l_3
l_{N-2}
l_{N-1}
l_N
Φ_1
Φ_2
Φ_3
Φ_{N-2}
Φ_{N-1}
Φ_N
s_1
d_1
s_2
d_2
s_3
s_{N-2}
d_{N-2}
s_{N-1}
d_{N-1}
s_N
x_1
x_2
x_3
x_{N-2}
x_{N-1}
x_N

Fig. 1

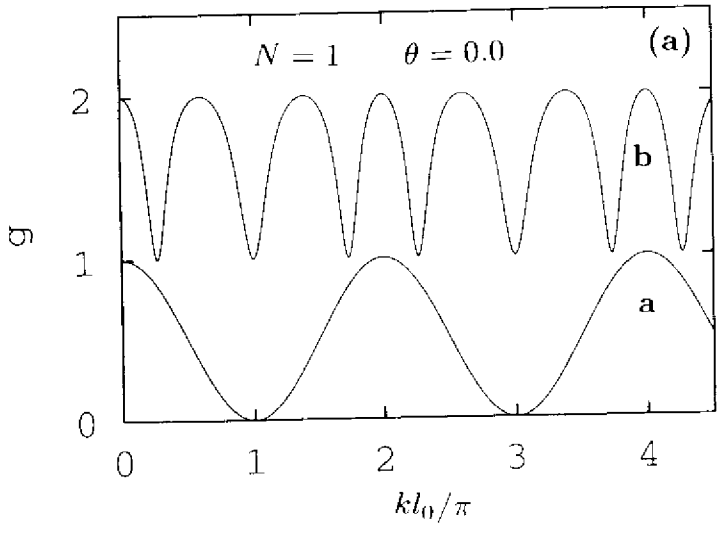
$N = 1$
$\theta = 0.0$
(a)
b
a
g
2
1
0
0
1
2
3
4
kl_0/π

Fig. 2a

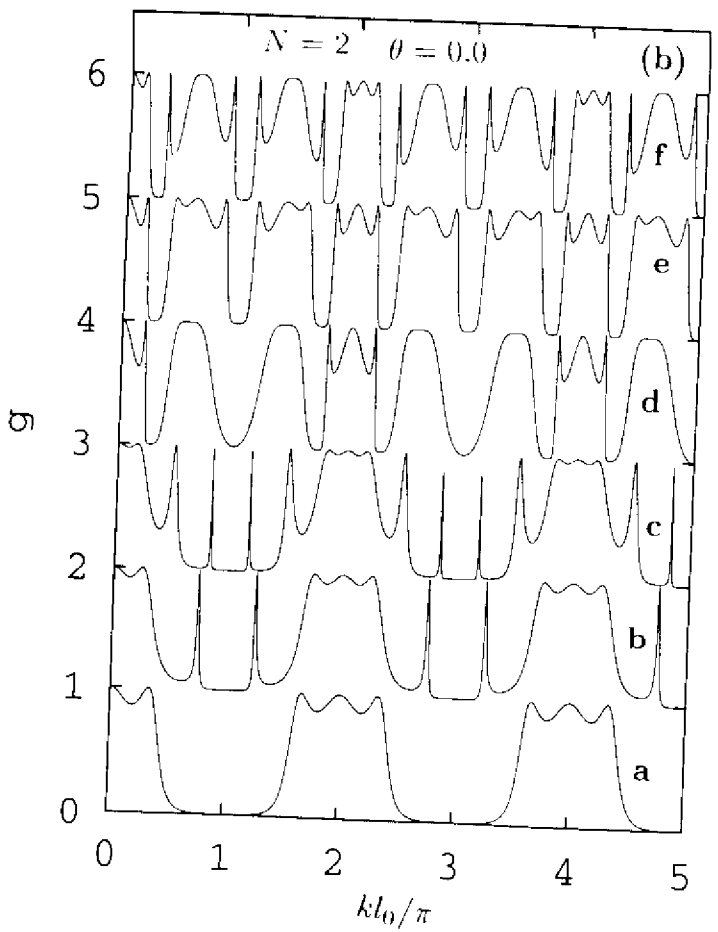

Fig. 2b

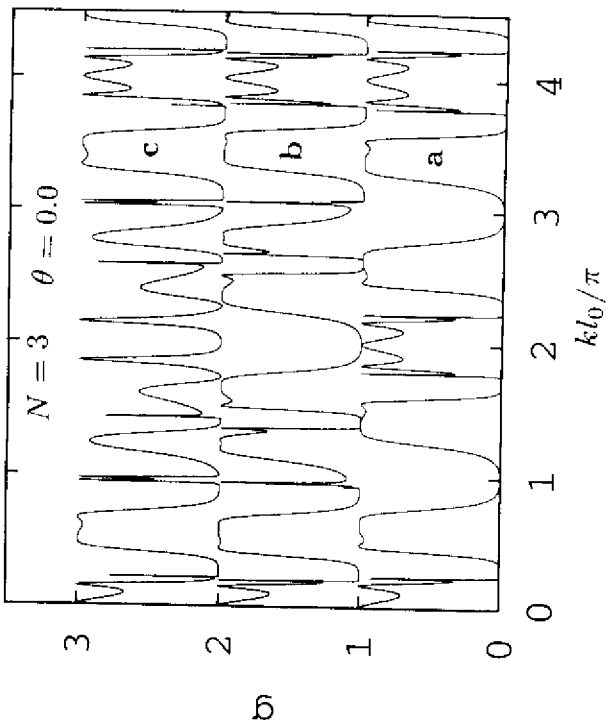

Fig. 3

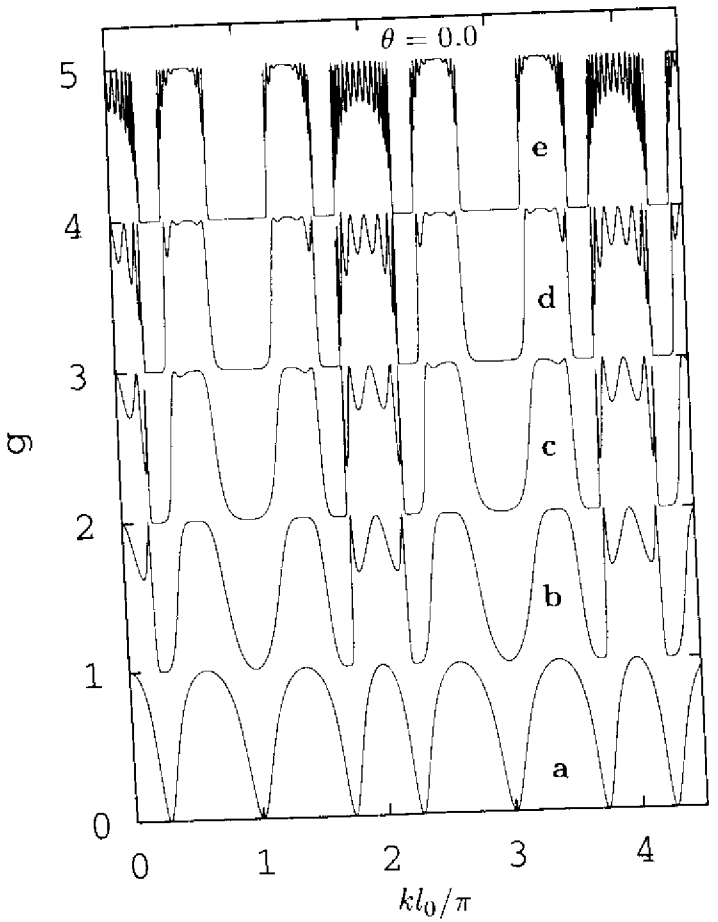

Fig. 4

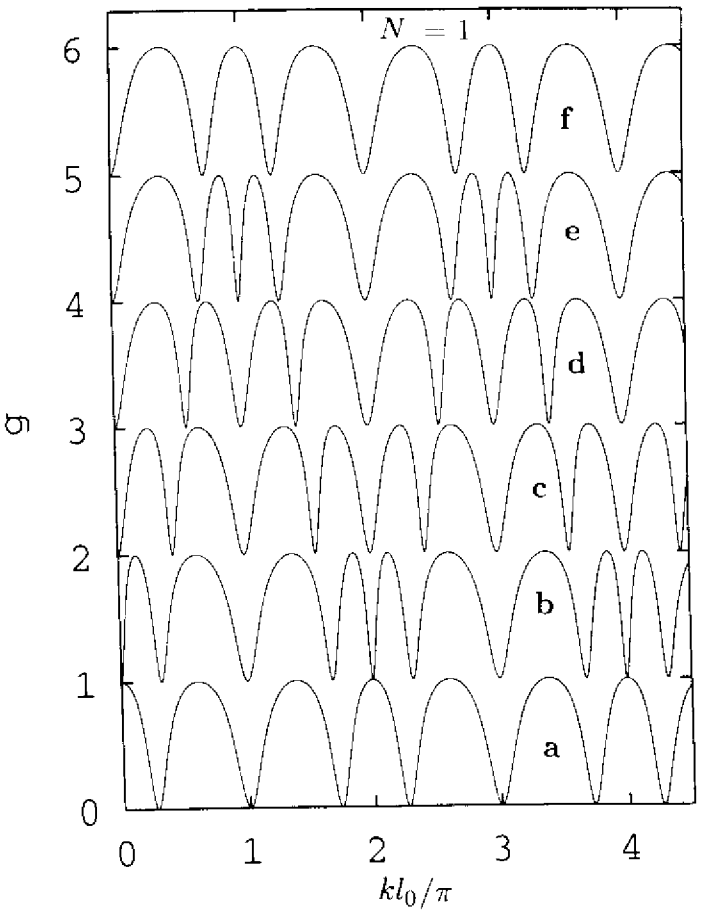

Fig. 5

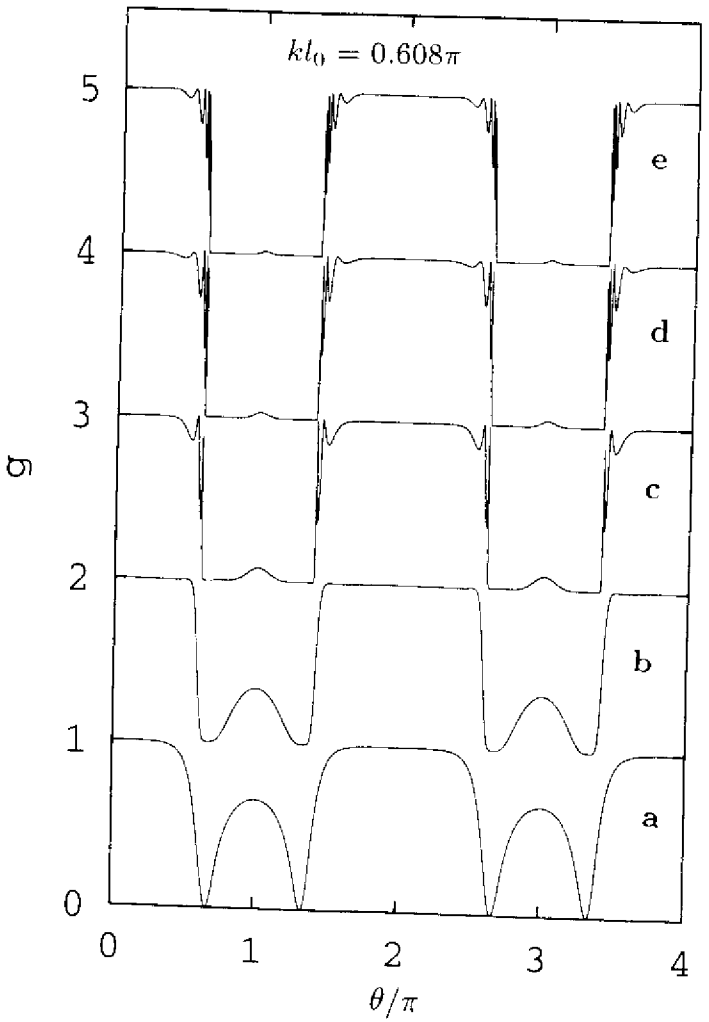

Fig. 6

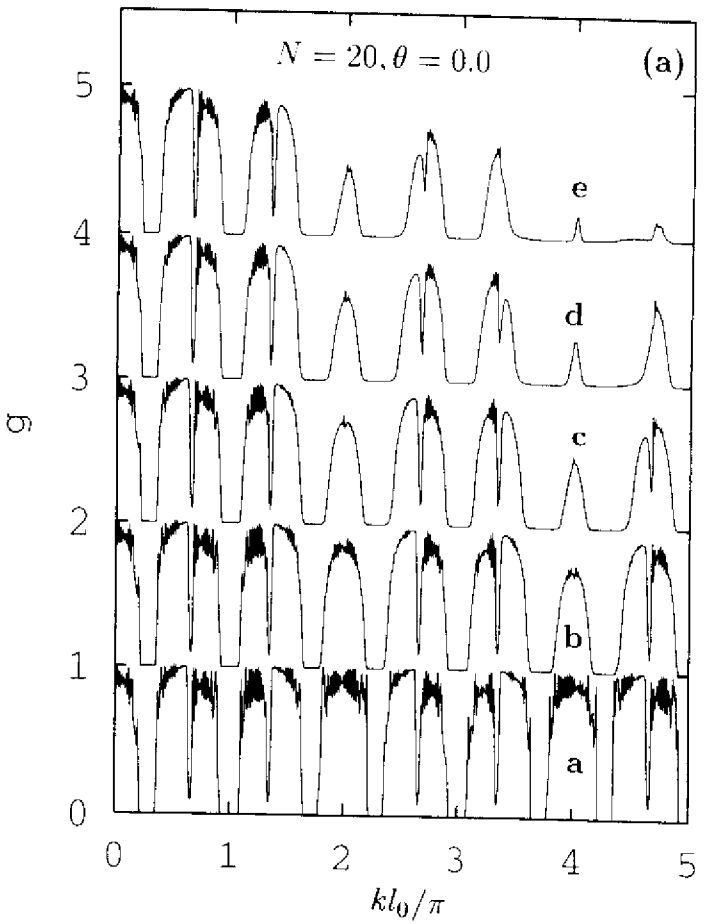

Fig. 7a

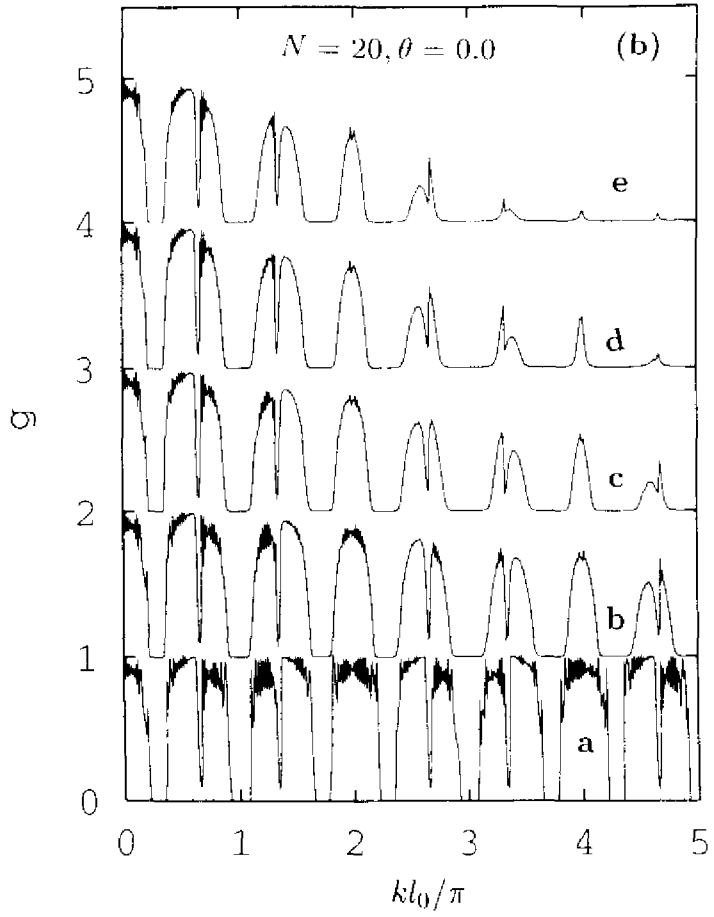
$N = 20, \theta = 0.0$
(b)
e
d
c
b
a
g
kl_0/π
0
1
2
3
4
5

Fig. 7b

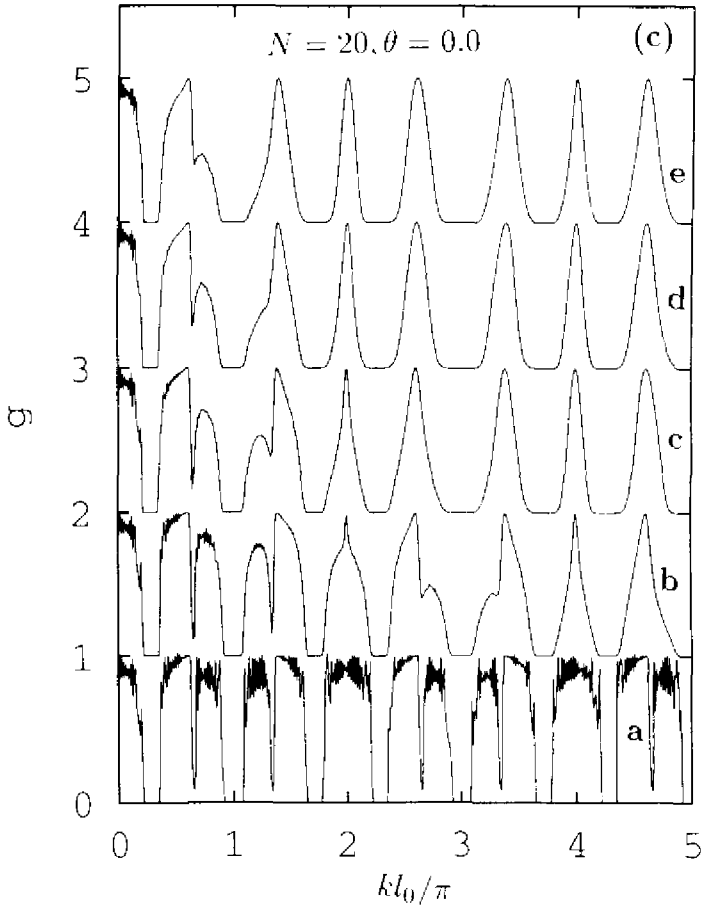
$N = 20, \theta = 0.0$
(c)
e
d
c
b
a
g
kl_0/π
0
1
2
3
4
5

Fig. 7c

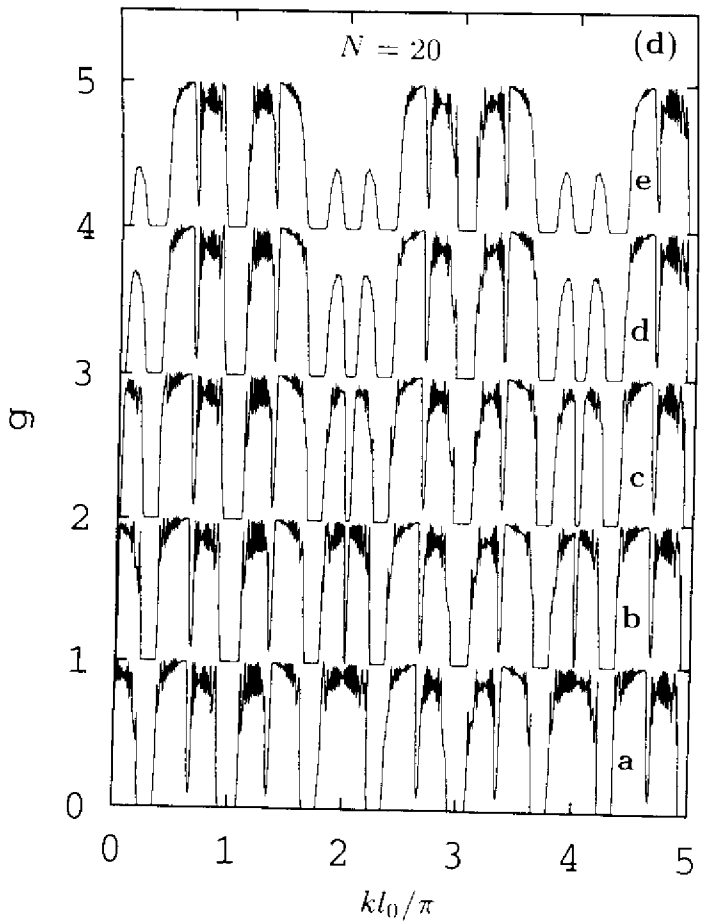

Fig. 7d